Multipurpose Monte Carlo simulator for photon transport in turbid media

Pedro Guerra, *IEEE Member,* Juan Aguirre, Juan E. Ortuño, Maria J. Ledesma-Carbayo, *IEEE Member*, Juan J. Vaquero, *IEEE Senior Member*, Manuel Desco and Andres Santos, *IEEE SeniorMember*

Abstract–**Monte Carlo methods provide a flexible and rigorous solution to the problem of light transport in turbid media, which enable approaching complex geometries for a closed analytical solution is not feasible. The simulator implements local rules of propagation in the form of probability density functions that depend on the local optical properties of the tissue.**

This work presents a flexible simulator that can be applied in multiple applications related to optical tomography. In particular, unlike previous codes, the simulator explicitly supports fluorescent-tissues and variance reduction and code parallelization techniques are implemented in order to speed up the execution with fluorochrome-labelled agents.

The simulator is validated with simple geometries for which an analytical solution exists, as well as with an experimental polyester resin based optical phantom.

I. INTRODUCTION

THE complicated nature of photon propagation in tissue makes the exact solution of the Maxwell's equations a very difficult endeavor. The radiative transfer equation (RTE), a differential equation describing radiance that is derived from energy conservation principles, is widely accepted as an accurate model for light propagation in tissues. [1]. However, the RTE does not have closed analytical solutions for arbitrary geometries and finite element methods (FEM) numerical solutions with sufficiently dense discretizations lead to computationally expensive problems. The RTE can also be solved with a Monte Carlo (MC) simulation by modeling local rules of propagation and tracking the fate of thousands of independent photons.

This work deals with photon transport simulation in a complex setup in which multiple light sources illuminates the sample and several detectors are placed around the object. The goal is to develop a flexible code capable of simulating diagnostic [2, 3] and therapeutic [4] applications, with particular emphasis on optical tomography, either diffuse (DFOT) [5, 6], or projective [7]. Fluorescence optical tomography (FOT), is a particular case of DFOT, where the aim is to retrieve the localization of fluorochrome-labeled agents. The presence of these molecules, leads to revisiting existing codes, such as MCML [8], in order to incorporate the physical process of light absorption by the fluorochromes and later reemission at a longer wavelength.

The document presents the physical model that has been considered, outlines the execution kernel of the simulator and present some validation results.

II. MATERIAL AND METHODS

A. Physics Model

1) Photon Description

Photons are described by the following variables: weight (w), the current spatial coordinates (X), time (t), its current wavelength (λ), the photon local axes coordinates $C'=(i',j',k')$, being k' also the propagation vector U, and current location within the voxellized tissue. Cartesian coordinates are preferred because in this case formulas for propagation are simpler [9], and the angle variables describing photon direction do not change unless the photon's direction changes.

2) Tissue Model

The object is discretized into voxels, each of which is represented by tissue type and fluorescent properties, resulting the tuple (μ_a, μ_s, g, n, μ_{af}, Φ), that correspond with the absorption coefficient (cm^{-1}), the scattering coefficient (cm^{-1}), the anisotropy factor, the index of refraction, the fluorophore absorption coefficient (cm^{-1}) and the fluorophore quantum yield respectively. Biological tissues in the near infrared (NIR) range are strongly forward scattering with anisotropy factors typically in the range 0.69< g <0.99.

3) Fluorochrome Model

A fluorophore is a component of a molecule which causes a molecule to be fluorescent: absorbs photons at wavelength λ_i and re-emits them at a longer wavelength λ_f. The emission wavelength λ_f is independent of the excitation wavelength; however the efficiency of this energy transfer, quantum efficiency Φ, does depend on λ_i. Moreover, the time required for the molecule to relax and return to ground state, thus emitting a photon at λ_i, is characteristic of each fluorochrome.

There is no limitation in the number of fluorescent agents than can be attached to tissue types; thus enabling different concentrations and types of fluorescent-dyes. There is also no constraint in the absorption and emission spectrum of the fluorochromes, though current simulations assume a constant yield and a monochromatic reemission.

In case of using different dyes, crosstalk effects are by construction part of the simulation.

4) Photon-matter interaction

At each interaction point C, a photon p may either interact with the tissue or a fluorophore. In the former case the photon is either absorbed or scattered while in the later case the photon is either absorbed by the fluorophore or reemitted at a longer wavelength. Tissue and fluorophore properties may be lumped together [10] to define an equivalent attenuation coefficient μ_{ac} and yield Φ_{ac} :

$$\mu_{ac} = \mu_a + \mu_{af}$$
$$\mu_{sc} = \mu_a \qquad\qquad (1)$$
$$\Phi_c = \frac{\mu_{af}}{\mu_a + \mu_{af}} \cdot \Phi$$

These definitions are convenient for obtaining the probably of each of the possible outcomes of the photon-matter interaction: scattering (p_s), absorption in tissue or fluorochrome (p_a) and fluorochrome absorption-remission (p_{ef}), which are given by:

$$p_s = \frac{\mu_s}{\mu_{ac} + \mu_s}$$
$$p_a = \frac{\mu_{ac}}{\mu_{ac} + \mu_s} \cdot (1 - \Phi_c) \qquad\qquad (2)$$
$$p_{ef} = \frac{\mu_{ac}}{\mu_{ac} + \mu_s} \cdot \Phi_c$$

In an ideal MC implementation, a coin would be tossed to determine the photon fate and in case of absorption, photon dies and a new photon is taken from the laser. This work considers forced interactions in order to reduce variances. This approach implies that at each interaction the photon packet is split into three fractions, each of which undergoes on of the possible processes. From a practical perspective, the consequence of this approach is that at tissue voxels labeled with fluorochromes, the initial photon packet splits in two: one that represents the fraction of photons that undergo scattering and the other the fraction of absorbed photons that are reemitted by the fluorophore. The simulator kernel handles this situation by placing the reemitted photon in a queue for later simulation and continuing the simulation with the scattered photon.

Whenever a photon is absorbed by the tissue and reemitted at a different wavelength, tissue property tables are updated accordingly, this procedure overcomes the limitations of other simulation codes [9].

5) Photon scatering

The differential scattering cross section is referred to as the phase function $p(\theta, \varphi)$, which specifies the probability of scattering into a unit solid angle (θ, φ), measured from the incident direction. The average over the solid angle of $p(\theta, \varphi)$ is known as the asymmetry parameter, which ranges from backward (g=-1) to forward scattering (g=1). A photon is considered to acquired random direction after approximately $1/(1-g)$ scatters. The Henyey-Greenstein phase function [11] is used to characterize the angular distribution of scattered light by tissue. This function is parameterized by the average cosine of the scattering angle $<\cos(\theta)>$, i.e. the anisotropy factor g:

$$p_{HG}(\cos\theta) = \frac{1}{2} \cdot \frac{1 - g^2}{\left(1 + g^2 - 2 \cdot g \cdot \cos\theta\right)^{\frac{3}{2}}} \qquad (3)$$

6) Photon mechanics

Photon mechanics involves translations due to propagation as well rotations due to scattering, reflection or refraction at tissue interfaces. Photon local axes are defined such that B_c represents the matrix transformation between the local reference system **C'** and the world reference system **C** and the propagation vector in the world system U aligns with the k'-axis in the local reference frame. That is,

$$U_L = (0, 0, 1)^T$$
$$U = B_c \cdot U_L \qquad\qquad (4)$$

With this definition, for a photon located at $X=(x, y, z)$ traveling a distance Δs in the direction $U=(u_x, u_y, u_z)$, the new coordinates X'=(x', y', z') are given by:

$$X^{(i+1)} = X^{(i} + \Delta s \cdot B_c \cdot U_L \qquad (5)$$

Reflections and refraction take place at the interface between two tissues; this interface is defined by the normal vector n. In both cases, the new direction of propagation U' belongs to the plane defined by U and n and it is computed as a rotation around the vector normal to the plane $S=Uxn$. Rotations are implemented on the transformed system C' as a rotation R around S, as:

$$B_c^{(i+1)} = B_r \cdot R \cdot B_r^T B_c^{(i} \qquad (6)$$

Where the rotation matrix B_r is defined as $((nxS)^T, n, S^T)$. In the case of reflection the rotation angle will be $(p-2\alpha_V)$ while in the case of refraction it will be $(a_{V'}-a_V)$.

Photon-matter scattering inside the voxel is represented as deflection angle θ and a azimuth angle φ, with respect to the propagation direction $U=(u_x, u_y, u_z)$. This rotation transforms the photont reference vectors:

$$B_d = \begin{pmatrix} \dfrac{u_x \cdot u_z}{s_z} & -\dfrac{u_y}{s_z} & u_x \\[2mm] \dfrac{u_y \cdot u_z}{s_z} & \dfrac{u_x}{s_z} & u_y \\[2mm] -s_z & 0 & u_z \end{pmatrix} \cdot \begin{pmatrix} \cos\Phi\sin\theta \\ \sin\Phi\sin\theta \\ \cos\theta \end{pmatrix} \quad (7)$$

$$s_z = \sqrt{1 - u_z^2}$$

$$B_c^{(i+1)} = B_d \cdot B_c^{(i} \quad\quad (8)$$

7) Physical Data Collection

During the simulation several physical parameters are recorded, for both injected photons at wavelength λ_i as well as the reemitted photons at wavelength λ_F are measured, including reflectance, transmittance and fluence. Photon packet weights are normalized to the laser wavelength λ_i in order to represent energy.

At each interaction point the absorbed energy is stored in a matrix $\mathbf{A_{xyz}}$, which represents the total deposited energy at each voxel and it is proportional to the photon fluence $\Phi(r,\lambda)$. Fluence is computed out of the absorbed energy, adjusting for a scale parameter in order to fulfill that the exiting photon flux, consisting of total transmittance T_t and total radiance T_r, plus the absorbed energy at different wavelengths, $\Phi(r,\lambda)\mu(r,\lambda)$ equals the injected energy E [12]:

$$T_t + T_r + \sum_\lambda \sum_{Volumen} \Phi_{xyz}(r,\lambda)\cdot\mu_a(r,\lambda)\cdot V_{voxel} = E \quad (9)$$

B. MC Simulator kernel

1) Tools

The simulator has been coded in C++, threaded for multiprocessor environments with OpenMP 3.0 [13] and compiled with Intel Compiler 11.0 (Intel Corp., 2200 Mission College Blvd Santa Clara, CA, USA).

2) Kernel Core

The simulator follows an execution flow similar to that describe by Wang [8], with the added feature that tissues may be labeled with fluorochromes, something that was not possible with previous codes [9]. Additionally the simulator is fully extended to 3D and tracks photon timing and rotations enabling intensity modulated simulations and polarization considerations. For each photon packet, the following steps are carried out:

1. Select the photon for simulation, which may come from the queue previously mentioned or from the laser.
2. Update tissue tables to reflect properties at the current wavelength.

3. Compute the distance before the interaction point and translate the photon. Displacement may be such that more than one voxel is crossed. This requires updating the actual distances to reflect variations in tissue properties.
4. Compute the photon fraction that undergoes absorption, scattering and reemission. Store the reemission factor in the queue if its weight is higher than 0.
5. Apply Russian roulette to the photon: if its weight is lower than a given threshold a coin is tossed to determine whether the photon is absorbed or its weight is increased.
6. Iterate through steps 3-5 until the photon escapes the voxellized volume or it is completely absorbed.
7. Check whether the photon impinges on the external detectors.

III. RESULTS

A. Simulator validation against analytical solutions

The diffusion approximation (DA) equation [9] and data from existing literature is used to validate the code with simple slab geometries [14, 15]. Firstly, estimated observable physical values of the total reflectance and transmittance provided by the simulator is checked against published literature. The match of the results, summarized in the next tables, confirms the correctness of data scale factors and photon weightings.

TABLE 1: REFLECTANCE AND TRANSMITTANCE FOR A SEMI-INFINITE BLOCK

Author	R	R error	T	T error
Giovanelli [16]	0.26000	-	0	0
Prahl . [17]	0.26079	0.00079	0	0
Wang et al [8]	0.25907	0.00170	0	0
This work	0.25936	0.00142	0	0

TABLE 2: REFLECTANCE AND TRANSMITTANCE FOR A SLAB BLOCK

Author	R	R error	T	T error
van de Hulst [18]	0.09739	-	0.66096	
Prahl [17]	0.09711	0.00033	0.66159	0.00049
Wang et al [8]	0.09734	0.00033	0.66096	0.00020
This work	0.0969	9.43×10^{-4}	0.66160	0.00120

Next, the estimated photon fluence $\Phi(r,\lambda)$ is compared with the value provided by the DA for a slab geometry of thickness L=4 cm when taking into account the attenuation profile of the tissue [19].
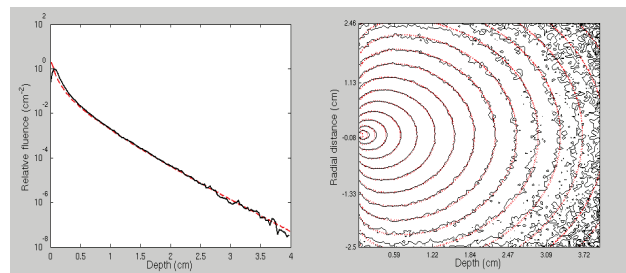

Figure 1: Longitudinal profile and axial cut of the fluence computed with the MC simulator and with the DA.

Figure 2 shows the fluence profile and a slice cut in logarithmic scale along the laser axis for the MC simulation

(solid line), with $5*10^7$ photons, and the DA analytical solution (dotted line) for a 4 cm slab geometry with the following optical parameters: $\mu_a=0.3$ cm-1, $\mu_s=100$ cm^{-1}, $g=0.9$, $D=0.033$ cm. As expected, except in points close to the surface where the laser impinges the tissue, there is complete correspondence between both solutions

B. Simulator validation against experimental data

The Monte Carlo simulator is validated against real measurements with an optical phantom. The scattering coefficient and the absorption coefficient of the phantom can be tuned according to the concentration of absorber and scatterers [20]. For the studies presented herein we made several phantoms using polyester resin as bulk matrix, Pro-Jet ink 900 NP (ICI plc., Slough, UK) as absorber and TiO_2 as scatterer [20] whose optical parameters are $(\mu_a, \mu_s, g)=(0.1$ cm^{-1}, 8 cm^{-1},0.9).
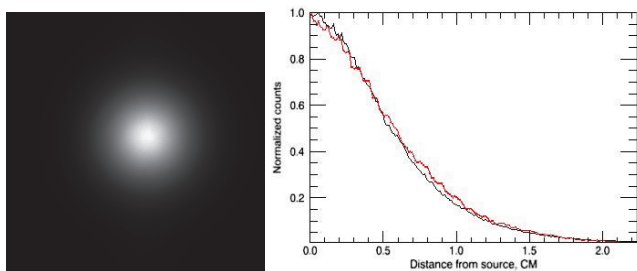

Figure 2: Experimental laser spot on the detector (left) and radial profile of the experimental spot and the MC simulation output when illuminating the resin phantom.

IV. CONCLUSIONS AND FUTURE WORK

This work has presented a MC simulator for the transport of light in biological tissue that explicitly supports fluorescent activity inside the tissue. This feature enables the simulation of optical tomographs with complex structures, such as small animal phantoms and will provide a way to better understand photon propagation issues and thus optimize reconstruction algorithms. Moreover, the integration of fluorescence in the simulator enables the simulation of second-order effects, such as crosstalk between dyes and variations of optical tissue properties with wave length, that are usually neglected by analytical solutions.

Further validation with fluorochrome sources is in progress as well as an assessment of actual speed up achieved with the implemented multiprocessor threading.

REFERENCES

[1] O. Dorn, "A transport-backtransport method for optical tomography," *Inv. Probl.,* vol. 14, no. 5, pp. 1107-1130, 1998.

[2] S. K. Chang, D. Arifler, R. Drezek *et al.*, "Analytical model to describe fluorescence spectra of normal and preneoplastic epithelial tissue: comparison with Monte Carlo simulations and clinical measurements," *Journal of Biomedical Optics,* vol. 9, no. 3, pp. 511, 2004.

[3] I. Pavlova, C. R. Weber, R. A. Schwarz *et al.*, "Monte Carlo model to describe depth selective fluorescence spectra of epithelial tissue: applications for diagnosis of oral precancer," *Journal of Biomedical Optics,* vol. 13, no. 6, pp. 064012, 2008.

[4] L. H. P. Murrer, J. P. A. Marijnissen, and W. M. Star, "Ex vivo light dosimetry and Monte Carlo simulations for endobronchial photodynamic therapy," *Physics in Medicine and Biology,* vol. 40, no. 11, pp. 1807, 1995.

[5] D. A. Boas, D. H. Brooks, E. L. Miller *et al.*, "Imaging the body with diffuse optical tomography," *Signal Processing Magazine, IEEE,* vol. 18, no. 6, pp. 57, 2001.

[6] R. B. Schulz, J. Ripoll, and V. Ntziachristos, "Noncontact optical tomography of turbid media," *Opt. Lett.,* vol. 28, no. 18, pp. 1701, 2003.

[7] M. A. Haidekker, "Optical transillumination tomography with tolerance against refraction mismatch," *Computer Methods and Programs in Biomedicine,* vol. 80, no. 3, pp. 225, 2005.

[8] L. Wang, S. L. Jacques, and L. Zheng, "MCML--Monte Carlo modeling of light transport in multi-layered tissues," *Computer Methods and Programs in Biomedicine,* vol. 47, no. 2, pp. 131, 1995.

[9] T. J. Pfefer, J. Kehlet Barton, E. K. Chan *et al.*, "A three-dimensional modular adaptable grid numerical model for light propagation during laser irradiation of skin tissue," *Selected Topics in Quantum Electronics, IEEE Journal of,* vol. 2, no. 4, pp. 934, 1996.

[10] Q. Liu, C. Zhu, and N. Ramanujam, "Experimental validation of Monte Carlo modeling of fluorescence in tissues in the UV-visible spectrum," *Journal of Biomedical Optics,* vol. 8, no. 2, pp. 223-236, 2003.

[11] L. G. Henyey, and J. L. Greenstein, "Diffuse radiation in the galaxy," *Annales d'Astrophysique,* vol. 93, pp. 70, 1941.

[12] D. A. Boas, J. P. Culver, J. J. Stott *et al.*, "Three dimensional Monte Carlo code for photon migration through complex heterogeneous media including the adult human head," *Optics Express,* vol. 10, no. 3, pp. 159, 2002.

[13] OpenMP Architecture Review Board, *OpenMP Application Program Interface http://openmp.org*, 2008.

[14] R.C. Haskell, L.O. Svaasand, T.T. Tsay *et al.*, "Boundary-Conditions For Diffusion Equation in Radiative- Transfer," *J. Opt. Soc. Am. A - Optics Image Science and Vision,* vol. 11, pp. 2727-2741, 1994.

[15] M. S. Patterson, B. Chance, and B. C. Wilson, "Time resolved reflectance and transmittance for the non-invasive measument of tissue optical properties," *Applied Optics,* vol. 28 (12), pp. 2331-2336, 1989.

[16] R. G. Giovanelli, "Reflection by Semi-infinite Diffusers," *Journal of Modern Optics,* vol. 2(4), pp. 153, 1955.

[17] S. A. Prahl, M. Keijzer, S. L. Jacques *et al.*, "A Monte Carlo Model of Light Propagation in Tissue," *SPIE Institute Series,* vol. 5, pp. 102, 1989.

[18] H. C. van de Hulst, *Light Scattering by Small Particles*: Dover, 1981.

[19] A. Garofalakis, G. Zacharakis, G. Filippidis *et al.*, "Characterization of the reduced scattering coefficient for optically thin samples: theory and experiments," *Journal of Optics A: Pure and Applied Optics,* vol. 6, pp. 725, 2004.

[20] B. W. Pogue, and M. S. Patterson, "Review of tissue simulating phantoms for optical spectroscopy, imaging and dosimetry," *Journal of Biomedical Optics,* vol. 11, no. 4, pp. 041102, 2006.